Mineralogy and Petrology (2004) 81: 19–41
DOI 10.1007/s00710-003-0021-5

Mineralogy and Petrology
Printed in Austria

Late Neoproterozoic strongly peraluminous leucogranites, South Eastern Desert, Egypt – petrogenesis and geodynamic significance

A. M. Moghazi[1], **M. A. Hassanen**[1], **F. H. Mohamed**[1], and **S. Ali**[2]

[1] Geology Department, Faculty of Science, Alexandria University, Alexandria, Egypt
[2] Faculty of Earth Sciences, King Abdulaziz University, Jeddah, Saudi Arabia

Received March 31, 2003; revised version accepted September 24, 2003
Published online February 17, 2004;
Editorial handling: *J.G. Raith*

Summary

Late Neoproterozoic garnet-bearing leucogranites are developed locally along thrust faults in the South Eastern Desert, Egypt. This work presents field observations, whole rock major and trace element abundances, Rb–Sr isotope data and mineral chemistry for three occurrences in the Sikait-Nugrus area. Field observations show that the leucogranites cut the faults and their contact with the country rocks is sharp with no indication of contact metamorphism. They were intruded into a low-grade metamorphosed ophiolitic melange and a high-grade metamorphosed metasedimentary succession of biotite schist composition. Numerous biotite schist enclaves, having irregular and diffuse contacts, are recorded within the leucogranites. Whole rock Rb–Sr ages of the leucogranites from two different localities are 610 ± 20 and 594 ± 12 Ma respectively; they are interpreted as emplacement ages. The leucogranites contain more than 70% SiO_2, and they are strongly peraluminous ($A/CNK > 1.1$) with low TiO_2, $Fe_2O_3{}^*$, MgO, CaO, Ba, Sr, LREE, Eu/Eu^* and Sr/Ba and high Rb, Rb/Zr, Rb/Sr and Rb/Ba. These geochemical parameters and the low initial $^{87}Sr/^{86}Sr$ ratios ($\sim$0.703) indicate crustal derivation by dehydration partial melting from a juvenile protolith similar to the exposed biotite-rich metasediments. Models for the tectonic setting of these leucogranites suggest their emplacement during an extensional tectonic stage that follows continental collision. It is proposed that crustal heating, caused by decompression along shear zones, is responsible for the production of these granitic melts. The results support previous hypotheses and further document a regional late Neoproterozoic extensional tectonic event, which is probably related to the initial break-up of Gondwana.

Introduction

Granitoids display great diversity in their origin, sources and evolution processes and thus can be used as indicators of geodynamic environments and, in some cases as tracers of geodynamic evolution (*Barbarin*, 1999). The Neoproterozoic mobile belts of the Arabian-Nubian Shield (ANS) have been recognized as a typical example of an accretionary orogen defined by juvenile terranes. They yield Neoproterozoic Nd model ages (*Stern*, 2002) and have experienced a complete Wilson cycle (*Stern*, 1994). Compared with other collisional orogenic belts, the ANS is characterized by the emplacement of large volumes of felsic magmas of various compositions. In Egypt, granitoids constitute about 50% of the basement complex. Two main granite types are distinguished, i.e. older and younger granitoids (*Akaad* and *Noweir*, 1980). The older granitoids range in composition, from quartz diorite to granite (predominantly trondhjemite, tonalite and granodiorite). They are calc-alkaline I-type granites that were emplaced during active subduction processes between 870 and 614 Ma (*Stern* and *Hedge*, 1985; *Hassan* and *Hashad*, 1990;

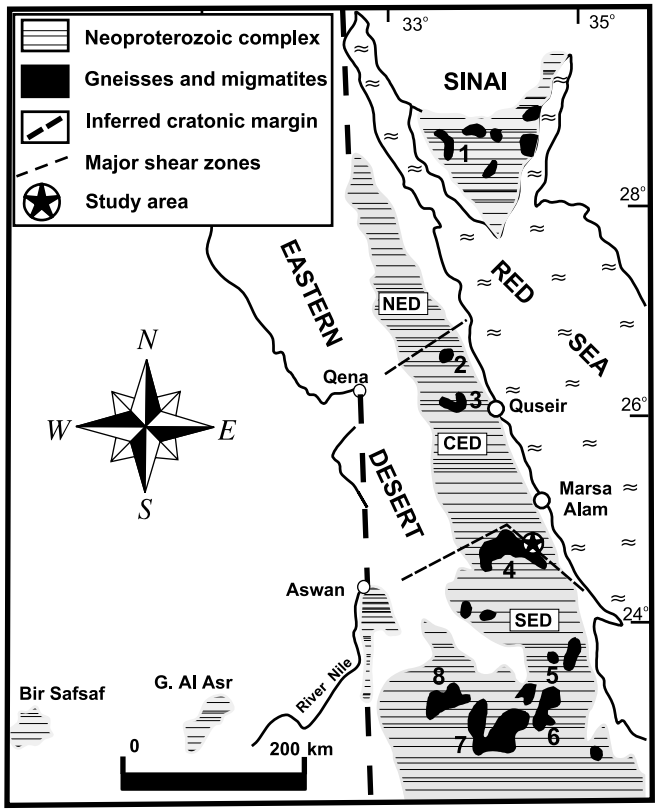

Fig. 1. Simplified map of Egypt with distribution of gneisses and migmatites (modified from *Hassan* and *Hashad*, 1990). Inferred cratonic margin is from *Sultan* et al. (1992). The shear zones separating north Eastern Desert (NED), central Eastern Desert (CED) and south Eastern Desert (SED) are from *Stern* and *Hedge* (1985). The areas indicated by numbers are: *1* Feiran-Solaf belt, *2* Um Had, *3* Gabal Meatiq, *4* Migif-Hafafit area, *5* Wadi Khuda, *6* Wadi Hodein, *7* Bir Haymur, *8* Abu Swayel. Asterisc marks the study area

Stern, 1994; *Kröner* et al., 1994; *Moghazi*, 1999). The younger granitoids are predominantly red to pink A-type granites (monzogranite, syenogranite and alkali feldspar granite), which were emplaced during a post-orogenic period between 610 and 550 Ma (*Stern* and *Hedge*, 1985; *Beyth* et al., 1994; *Moghazi*, 1999). On the other hand, some high-grade metamorphic domains in the Eastern Desert and Sinai represented by gneisses and migmatites (Fig. 1) contain leucogranite veins and sheets. These leucogranites have been used to date the peak of metamorphism (*El Ramly* et al., 1984; *Kröner* et al., 1988). Some other gneisses and migmatites are associated with small strongly peraluminous leucogranite plutons that intruded into metasediments (*Ragab* and *El-Gharabawi*, 1989; *Mohamed* and *Hassanen*, 1997; *Moghazi* et al., 2001). Although strongly peraluminous leucogranites are of limited distribution in the Egyptian Shield, their close spatial association with gneisses and migmatites is important. They may be used to relate high-grade metamorphism and magmatism with tectono-metamorphic events in the Eastern Desert of Egypt.

In the present paper, whole rock Rb–Sr isotopic data, geochemical and mineral chemistry data of leucogranites and metasediments from the Sikait-Nugrus area in SE Egypt (Fig. 1) are presented. The aim is to infer a specific geodynamic environment of the granitoids and to discuss their genesis in relation to the geodynamic evolution of the ANS.

Geological setting

General geological background and previous studies

The basement rocks in the Eastern Desert of Egypt represent a typical example of an accretionary orogen, which were evolved during the Neoproterozoic from a number of island-arc and back-arc basin systems (*Kröner*, 1985; *Stern*, 1994). These arc terranes developed during Neoproterozoic times (i.e. between ca. 870 and 650 Ma) in an oceanic environment (*Kröner* et al., 1992; *Stern*, 1994) and offshore of the Saharan Metacraton (*Abdelsalam* et al., 2002), which constitutes the basement rocks west of the river Nile (Fig. 1). This tectonic evolution from oceanic lithosphere to island-arcs and continental lithosphere is well documented by the rock sequences (e.g. ophiolite suites, ocean floor sedimentary sequences, island arc volcano-sedimentary association, and calc-alkaline I-type intrusive igneous rocks) constituting the ANS. The Neoproterozoic orogeny culminated with the collision between East and West Gondwana (*Stern*, 1994; *Meert*, 2003). A-type granites (younger granites) and related volcanic rocks (Dokhan Volcanics) and molasse-type sediments (Hammamat Group) are the main rock units formed in the post-collision stage (*Stern* and *Gottfried*, 1986; *Willis* et al., 1988; *Moghazi*, 2003; *Jarrar* et al., 2003).

Recently, the Eastern Desert of Egypt is considered to be composed of a number of gneissic domes (or core complexes) exposed in a tectonic window through the Pan-African cover nappes, which include ophiolites and island-arc volcanic rocks (*Fritz* et al., 1996, 2002; *Loizenbauer* et al., 2001). The gneissic domes were referred to as ''infrastructure'' whereas the Pan-African nappes were referred to as ''suprastructure'' (*El Gaby* et al., 1990). They occur at Gabal Meatiq (*Sturchio*

et al., 1983; *Blasband* et al., 2000; *Fowler* and *Osman*, 2001; *Loizenbauer* et al., 2001), in three distinct domal structures in the Migif-Hafafit area (*El Ramly* et al., 1984; *Greiling* et al., 1988; *Rashwan*, 1991; *Fowler* and *El Kalioubi*, 2002), in the Abu Swayel area (*Finger* and *Helmy*, 1998), in the Wadi Haimur area (*Abd El Naby* and *Frisch*, 2002), in the Wadi El Hudi area (*Sultan* et al., 1994; *Moghazi* et al., 2001) and in southern Sinai at Wadi Feiran (*Stern* and *Manton*, 1987; *Kröner* et al., 1994). Core complex formation within the Eastern Desert of Egypt is closely linked with the NW-trending Najd Fault System (*Stern*, 1985). This dominantly sinistral strike-slip system strikes approximately parallel to the orogen over a distance of several hundreds of kilometers (*Fritz* et al., 2002). The core complexes (gneissic domes) occur along strike of the Najd Fault System (*Fritz* et al., 1996). Sinistral strike-slip shear zones determine the eastern and western dome margins whereas the northern and southern margins are defined by prominent normal faults (*Wallbrecher* et al., 1993). These structures are related to NW–SE compression with contemporary N–S extension that accommodated exhumation of these core complexes and emplacement of granitoid rocks (*Bregar* et al., 2002; *Fritz* et al., 2002).

The Migif-Hafafit core complex lies to the south of a major shear zone known as the Nugrus thrust fault (*Greiling* et al., 1988) or Nugrus strike-slip fault (*Fritz* et al., 2002). This shear zone separates high-temperature metamorphic rocks of the Hafafit complex in the SW from mainly low-grade ophiolitic and arc volcanic assemblages to the NE (*Bennett* and *Mosley*, 1987). The structural evolution of the Migif-Hafafit area has been described in detail by *El Ramly* et al. (1984), *Greiling* et al. (1988), *Rashwan* (1991), *Kröner* et al. (1994), *Fowler* and *El Kalioubi* (2002) and a structural evolutionary scheme involving many deformation phases has been suggested. These deformation phases led to a complex development of a series of anticlines and synclines, strike-slip and normal faults.

Geology of the study area

The study area lies along the NE margin of the Migif-Hafafit metamorphic core complex (Fig. 1). The rocks exposed (Fig. 2) are mainly metasediments, orthogneisses, ophiolitic mélange and garnet-bearing leucogranites. The metasediments and the orthogneisses occupy the area to the south of the major Nugrus fault as a part of the Hafafit core complex. The metasediments are represented by a thick succession of highly foliated garnetiferous mica schists of pelitic parentage, which show little evidence of preservation of sedimentary structures and textures. The orthogneisses are metadiorite (hornblende gneiss) and metagranodiorite to granite (biotite gneiss). These lithologies are coarse- to medium-grained, highly foliated and show weak to strong gneissic fabrics. In the weakly deformed varieties, igneous textures are well preserved. The ophiolitic mélange, which represents the hangingwall of the major Nugrus thrust, contains the most abundant rocks in the study area. They consist of a greenschist facies metamorphosed sedimentary matrix enclosing amphibolite sheets, allochthonous serpentinite and gabbroic masses and quartzite bands that range in size from less than a meter to several kilometers. They are considered as the continuation of the distal facies of the Wadi Ghadir ophiolitic mélange, which lies towards the northeast of the study area (*Hilmy* et al., 1990; *Takla* et al., 1992).

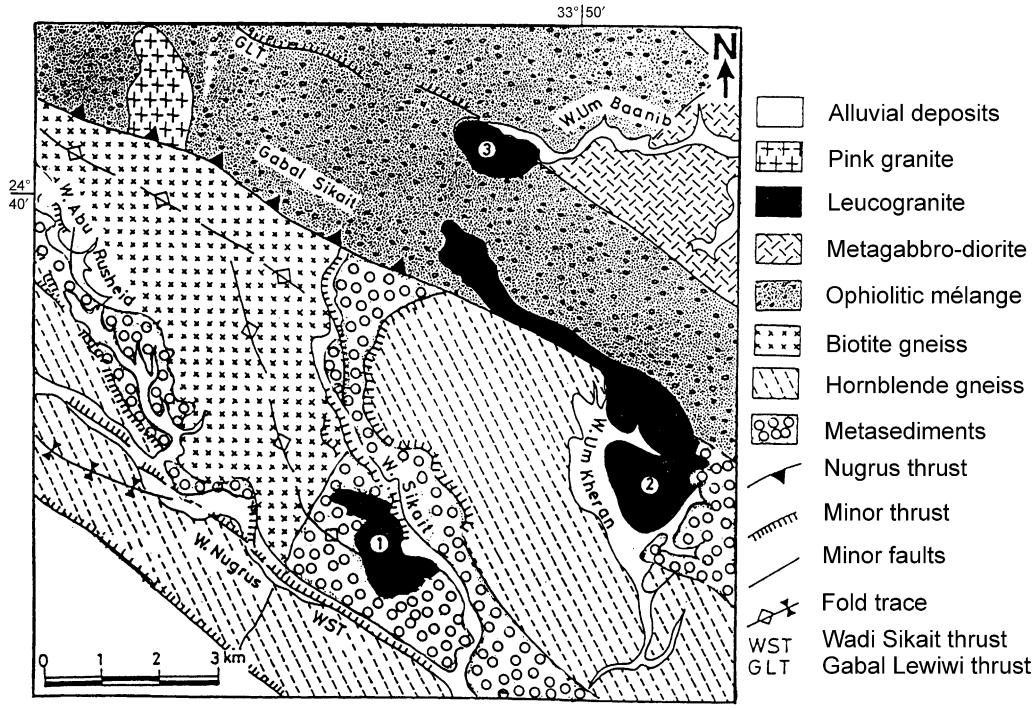

Fig. 2. Geological map of the Sikait-Nugrus area (modified from *Greiling* et al., 1988; *Mohamed* and *Hassanen*, 1997). The plutons investigated are indicated by numbers: *1* Sikait, *2* Um Kheran, *3* Um Baanib

The leucogranites form small lens-like plutonic masses at three distinct localities (Fig. 2). They are located within the Hafafit core complex in the footwall of the Nugrus fault (i.e. Wadi Sikait pluton), within the Neoproterozoic ophiolitic mélange in the hangingwall of the Nugrus fault (i.e. Wadi Um Baanib pluton) and along the contact of both units (i.e. Wadi Um Kheran pluton). The leucogranites are preferably found along minor and major faults. The leucogranite bodies cut the faults and their contact with the country rocks is clearly discordant and sharp with no indication of visible contact metamorphism. Most of these leucogranites are medium-to coarse-grained, garnet-bearing and contain abundant metasedimentary xenoliths. Occasionally, porphyritic leucogranite with large K-feldspar phenocrysts is observed. Limited weak deformations have been recorded within the leucogranites. While the central parts of the three plutons are massive and weakly deformed, their margins show evidence of limited foliation and lineation.

Analytical techniques

Major and trace element abundances from 37 samples (32 leucogranites and 5 metasediments) were determined using a Rigaku 3080EZ XRF instrument at the Institute of Geology, University of Tohoku, Japan. Major elements were determined using fused pellets, while trace element analyses were performed on pressed powder pellets. Rare earth element (REE) contents of 9 samples of the leucogranite

and metasediments were measured by ICP-MS analyses at the Federal Institute for Geosciences and Natural Resources, Hannover, Germany. Analytical precision is better than $\pm 3\%$ for major elements and ± 5 to $\pm 10\%$ for the trace and rare earth elements. The mineral chemical composition of some minerals from selected samples of metasediments and leucogranites were determined using a Hitachi X560S energy dispersive electron microanalyzer at Tohoku University, Japan.

The concentrations of Rb and Sr of 18 leucogranite and metasediment samples were determined by XRF techniques as decribed above. For evaluation of $^{87}Sr/^{86}Sr$ isotopic ratios, Sr was separated by standard ion exchange techniques and the $^{87}Sr/^{86}Sr$ ratios were determined using a thermal ionization mass spectrometer (VG Isomass 54E) at the Faculty of Earth Science, King Abdulaziz University, Jeddah. The $^{87}Sr/^{86}Sr$ ratios were normalized within-runs to $^{86}Sr/^{84}Sr = 0.1194$. The decay constant used for ^{87}Rb is 1.42×10^{-11} yr^{-1}. Age calculations have been carried out using the Isoplot 2.57 software package (*Ludwig*, 1991).

Petrography and mineral composition

Metasediments

Metasediments in the study area consist of two main types (Fig. 2): 1) low-grade mélange sediments in the hangingwall of Nugrus fault, which are mainly metamorphosed in the greenschist facies and contain pebbles of various composition, 2) high-grade metamorphosed sediments in the footwall of Nugrus fault. They are mainly mica schists characterized by a well-developed foliation. The average modes are: quartz (40%), plagioclase (20%), biotite (25%), K-feldspar (5%), garnet (3%), muscovite (3%), and chlorite (2%) with accessory apatite, zircon and tourmaline (2%). Quartz, plagioclase, and K-feldspar range in size from 0.1 to 0.6 mm. They occur as elongated grains or subhedral crystals stretched in the direction of foliation, which occasionally exhibit undulatory extinction or deformed twin lamellae. Biotite forms well-oriented 0.3–1 mm plates defining the strong foliation in the metasediments. Muscovite occurs as platy crystals (0.2–0.05 mm) mainly within some cleavage zones; it also occurs as lamellae intergrown with biotite. Garnet is either subhedral or anhedral with strongly embayed margins and contains abundant inclusions of quartz and biotite. Plagioclase is generally oligoclase to andesine (An_{17-30}). The composition of biotite is homogeneous, Fe-rich ($Fe/Fe + Mg = 0.71 - 0.74$) with 3.5–4.3 wt% TiO_2. The garnet is typically almandine-rich with the almandine components slightly increasing from core to rim (Table 1).

Leucogranites

The leucogranites consist of quartz (38%) plagioclase (32%), K-feldspar (20%), biotite (5%), garnet (4%) and muscovite (1%), Accessory minerals occur in very small proportions. Zircon is commonly present as inclusions in biotite. Magnetite and hematite are rare whereas apatite is mostly absent. Grain sizes are generally about a few millimeters and up to 5 mm, occasionally up to 1 cm within some dykes. Most samples are even-grained; a few are porphyritic with feldspar crystals up to 1 cm in length. Plagioclase (An_{15-19}) occurs as stubby subhedral

Table 1. *Representative mineral analyses for the Sikait-Nugrus leucogranites and metasediments*

	Garnet										Biotite						Muscovite	
	Schist		Leucogranite								Schist		Leucogranite				Leucogranite	
	SD-2		B854		K868			SI-11			S-2	S-3	B845	B854	K868	SI-11	B845	SI-11
	Rim	Core	Core	Rim	Core	Mid	Rim	Rim	Core									
SiO_2	36.14	36.68	37.78	37.37	37.26	37.23	37.29	37.43	37.19	SiO_2	34.22	34.83	34.96	35.59	34.97	35.35	45.23	45.43
TiO_2	0.06	0.00	0.00	0.00	0.00	0.00	0.00	0.08	0.12	TiO_2	3.61	4.26	0.31	0.62	0.23	2.38	0.64	0.66
Al_2O_3	20.85	21.23	21.81	21.74	21.49	22.00	21.47	21.60	21.36	Al_2O_3	16.82	16.88	20.03	20.47	20.42	19.75	33.81	32.93
Cr_2O_3	0.13	0.08	0.14	0.04	0.03	0.03	0.03	0.01	0.06	FeO	25.36	25.07	24.2	22.28	23.87	20.75	1.4	1.51
FeOt	30.27	28.85	26.48	28.39	27.28	26.81	26.96	27.30	27.24	MnO	0.28	0.28	0.21	0.27	0.19	0.15	4.06	3.47
MnO	4.87	4.93	2.36	2.04	4.20	2.36	1.88	1.89	1.91	MgO	5.53	5.04	7.91	7.33	7.9	9.32	0.19	0.23
MgO	2.74	2.13	3.45	3.14	2.13	3.55	3.42	3.68	3.38	Na_2O	0.2	0.28	0.36	0.48	0.16	0.26	0.51	1.09
CaO	4.62	5.76	9.18	8.61	8.41	8.91	9.08	8.74	8.85	K_2O	9.65	9.83	8.36	9.06	9.37	9.97	10.88	10.45
Total	99.55	99.58	101.20	101.34	100.80	100.88	100.13	100.72	100.10	Total	95.67	96.47	96.34	96.10	97.11	97.93	96.72	95.77
Alm	65.80	64.08	55.08	58.15	57.74	54.80	56.00	56.14	56.74	X_{phl}	0.23	0.21	0.30	0.29	0.31	0.36		
Grs	12.43	16.13	22.36	19.14	20.48	20.11	21.50	19.87	20.63	X_{sid}	0.56	0.56	0.60	0.62	0.61	0.54		
Prp	10.62	8.43	13.59	12.53	8.53	14.22	13.65	14.62	13.50	X_{ann}	0.21	0.23	0.09	0.09	0.08	0.10		
Sps	10.72	11.09	5.30	4.63	9.56	5.36	4.27	4.26	4.33	Fe_t/Fe_t+Mg	0.72	0.74	0.63	0.63	0.63	0.56	0.16	0.20

	K-feldspar						Plagioclase									
	Leucogranite				Schist		Leucogranite								Schist	
	B845	B854	K868	SI-11	S-3	S-4	B845	B854	K888	K889	K894	SI-11	SI-12AP	SI-3	S-3	S-4
SiO_2	65.55	65.14	65.1	65.35	63.35	63	63.13	62.39	63.41	64.33	63.89	62.85	63.03	62.97	63.25	61.61
Al_2O_3	18.6	18.19	18.71	18.51	18.8	18.99	22.63	22.53	22.51	22.82	22.56	23.04	22.8	22.49	22.42	24.68
CaO	0.1	0.03	0.1	0.1	–	–	3.92	3.23	3.69	3.35	3.35	3.64	3.73	3.83	3.46	5.7
Na_2O	0.65	0.74	0.63	0.67	0.12	0.44	9.22	9.6	9.34	9.69	9.67	9.51	9.57	9.12	9.18	7.74
K_2O	15	15.92	15	15.19	15.59	15.16	0.23	0.2	0.3	0.28	0.16	0.18	0.31	0.23	0.21	0.27
Total	99.9	100.02	99.54	99.82	97.86	97.59	99.13	97.95	99.25	100.47	99.63	99.22	99.44	98.64	98.52	100.1
Ab	6.1	6.6	6	6.2	1.2	4.2	79.9	83.4	80.7	82.6	83.2	81.7	80.9	80.1	81.7	69.9
An	0.5	0.1	0.5	0.5	–	–	18.8	15.5	17.6	15.8	15.9	17.3	17.4	18.6	17	28.5
Or	93.3	93.3	93.5	93.2	98.8	95.8	1.3	1.1	1.7	1.6	0.9	1	1.7	1.3	1.2	1.6

crystals with characteristic albite and Carlsbad twinning and appears to represent the earliest phase to crystallize from the granitic melt. In some samples, plagioclase has inclusions of small euhedral biotite crystals. Microcline is the common K-feldspar, which sometimes exhibit perthitic intergrowth. Garnet occurs as small well-developed crystals or slightly rounded grains with diameters of 1–5 mm, usually with tiny inclusions of biotite and quartz. Garnet is almandine-rich with spessartine component increasing and the pyrope component decreasing from core to rim (Table 1). Biotite in the leucogranites has less FeO and TiO_2 than the mica schists but is also Fe-rich with $Fe/Fe + Mg$ between 0.56 and 0.63. Muscovite is present as small platy crystals in variable amounts and is often intergrown with biotite. It is characterized by high proportions of TiO_2 (0.64–0.66%), MgO (3.37–4.06%) and Al_2O_3 (32.12–33.81%).

Geochemistry

Major and trace elements

Major and trace element data (Table 2) show no chemical differences between granite samples collected from the three occurrences (Sikait, Um Kheran, and Um Baanib). Thus all samples will be treated as a single leucogranite suite. All leucogranites are strongly peraluminous ($A/CNK = \text{molar } Al_2O_3/CaO + Na_2O + K_2O > 1.1$; Fig. 3A) with normative corundum values ranging between 0.22 and 5.4%. The strongly peraluminous character is also shown on the Al_2O_3/TiO_2 vs. CaO/Na_2O diagram (Fig. 3B), where the leucogranite samples are very similar to strongly peraluminous post-collision granites in other orogenic belts (*Sylvester*, 1998). In the CIPW-normative quartz–albite–orthoclase diagram (Fig. 3C), most of the Sikait-Nugrus leucogranite samples plot close to the minimum temperature area between 1 and 10 kb, and to the right of the cotectic/eutectic minima of the H_2O saturated haplogranite system, a common feature for low temperature granites (*Johannes* and *Holtz*, 1996; *Kalsbeek* et al., 2001). In Fig. 3D, the concentration of Zr in the Sikait-Nugrus leucogranites is compared to the proportions of Zr that can be dissolved in granitoid melts of various compositions at different temperatures (*Watson* and *Harrison*, 1983). The low concentrations of Zr in the studied leucogranites (<100 ppm in most samples, Fig. 3D) suggest relatively low temperatures of formation.

The leucogranites have between 71.7% and 77.6 wt% SiO_2 with moderate variations in Al_2O_3 (12.2–15.6%), $Fe_2O_3{}^*$ (0.08–1.8%), TiO_2 (0.01–0.25%), CaO (0.24–1.8%), MgO (0.02–0.54%), Rb (80–265 ppm), Sr (9–179 ppm), Zr (11–178 ppm), and Nb (2–50 ppm) (Table 2). Chemical analyses of the host metasediments illustrate compositional homogeneity of the sequence with values of Al_2O_3, CaO and Na_2O very similar to greywacke. The variation diagrams of some major and trace elements presented in Fig. 4 illustrate the compositional features of the leucogranites and the metasediments. In general, both lithologies define roughly linear arrays on most plots with the metasediments deviating towards the silica-poor end of this array. Relative to the metasediments, the leucogranites are rich in Rb and $Na_2O + K_2O$ and poor in CaO, $Fe_2O_3{}^*$, MgO, TiO_2, Cr, Sr and Zr.

Table 2. *Representative chemical analyses of Sikait-Nugrus leucogranites and metasediments*

Sample	Leucogranite						Metasediments			
	B846	B854	K870	K893	S10-IB	SII-B	SD-2	SD-3	SD-4	SD-5
SiO_2 wt%	73.76	71.72	73.52	72.79	77.55	72.26	69.72	70.32	68.52	67.5
TiO_2	0.21	0.17	0.24	0.18	0.04	0.01	0.61	0.59	0.65	0.55
Al_2O_3	14.47	14.06	14.64	14.42	14.50	15.77	14.06	13.40	15.83	15.81
Fe_2O_3*	1.53	1.53	1.73	1.32	1.11	1.02	5.10	6.81	4.72	5.04
MnO	0.06	0.05	0.05	0.06	0.20	0.24	0.09	0.07	0.08	0.11
MgO	0.54	0.41	0.36	0.40	0.14	0.07	1.47	1.50	1.63	2.15
CaO	0.70	1.73	1.76	1.68	0.57	1.57	1.40	1.54	2.3	2.18
Na_2O	3.04	2.97	3.27	3.08	2.65	4.73	3.97	5.14	3.56	3.3
K_2O	3.80	3.94	3.50	3.78	3.45	3.41	2.61	1.62	2.12	1.3
P_2O_5	0.06	0.05	0.05	0.06	0.03	0.01	0.09	0.22	0.15	0.18
LOI	1.12	2.44	0.63	1.54	1.37	0.62	1.16	1.02	1.54	2.22
Sum	99.29	99.07	99.75	99.31	101.61	99.71	100.28	102.23	101.1	100.34
A/CNK	1.39	1.14	1.18	1.18	1.59	1.10	1.18	1.03	1.28	1.46
Cr ppm	20	17	11	12	8	bd	31	39	40	65
Ni	11	12	11	10	7	bd	12	33	35	40
V	22	20	18	16	10	10	58	16	20	54
Cu	33	38	48	52	10	3	44	37	52	60
Pb	27	21	20	19	25	25	14	15	17	15
Zn	32	24	33	27	48	33	91	139	85	171
Rb	106	125	97	94	253	129	50	27	43	46
Ba	689	585	634	929	39	41	612	490	545	685
Sr	136	143	152	179	26	72	144	97	108	270
Ga	19	14	17	16	24	22	20	21	25	20
Nb	4	5	8	6	50	2	4	10	15	12
Zr	127	100	164	118	36	78	177	545	200	350
Y	18	15	22	16	9	141	11	108	64	42
Th	23	25	19	14	10	20	10	10	15	12
U	6	5	4	3	2	4	1	2	3	3
La	8.59	5.30	9.85	–	6.80	–	35.10	30.70	21.80	25.40
Ce	17.00	12.45	20.50	–	15.00	–	70.43	55.32	42.75	47.46
Pr	2.47	1.55	2.54	–	1.84	–	6.95	5.62	4.53	5.11
Nd	9.03	7.90	12.10	–	8.60	–	25.30	20.48	17.23	18.22
Sm	3.12	2.50	2.90	–	2.90	–	5.11	4.17	4.60	4.55
Eu	0.62	0.32	0.42	–	0.40	–	0.85	0.85	0.97	1.15
Gd	4.20	3.20	4.08	–	3.56	–	4.12	4.17	3.90	4.55
Dy	6.50	4.12	4.95	–	5.72	–	3.74	3.22	2.66	2.75
Ho	1.72	0.90	1.03	–	1.33	–	0.75	0.53	0.58	0.55
Er	4.00	2.65	3.05	–	3.77	–	2.10	1.56	1.28	1.50
Yb	4.95	2.96	3.33	–	3.64	–	2.33	1.49	1.30	1.80
Lu	0.72	0.48	0.49	–	0.65	–	0.30	0.19	0.15	0.25
Σ REE	68	49	69	–	56	–	158	130	105	116
La/Yb	1.17	1.21	2.00	–	1.26	–	10.18	13.92	11.33	9.54
Gd/Yb	0.69	0.88	0.99	–	0.79	–	1.43	2.27	2.43	2.05

(*continued*)

Table 2 (*continued*)

Sample	Leucogranite						Metasediments			
	B846	B854	K870	K893	S10-IB	SII-B	SD-2	SD-3	SD-4	SD-5
Eu/Eu*	0.52	0.35	0.37	–	0.38	–	0.57	0.62	0.70	0.77
Rb/Sr	0.78	0.87	0.64	0.53	9.73	1.79	0.35	0.28	0.40	0.17
Rb/Ba	0.15	0.21	0.15	0.10	6.49	3.15	0.08	0.06	0.08	0.07
Sr/Ba	0.20	0.24	0.24	0.19	0.67	1.76	0.24	0.20	0.20	0.39
Rb/Zr	0.83	1.25	0.59	0.80	7.03	1.65	0.28	0.05	0.22	0.13

*Fe_2O_3** total Fe as Fe_2O_3; *bd* below detection limit; – = not determined; *B* Baanib; *K* Um Kheran; *S* Sikait

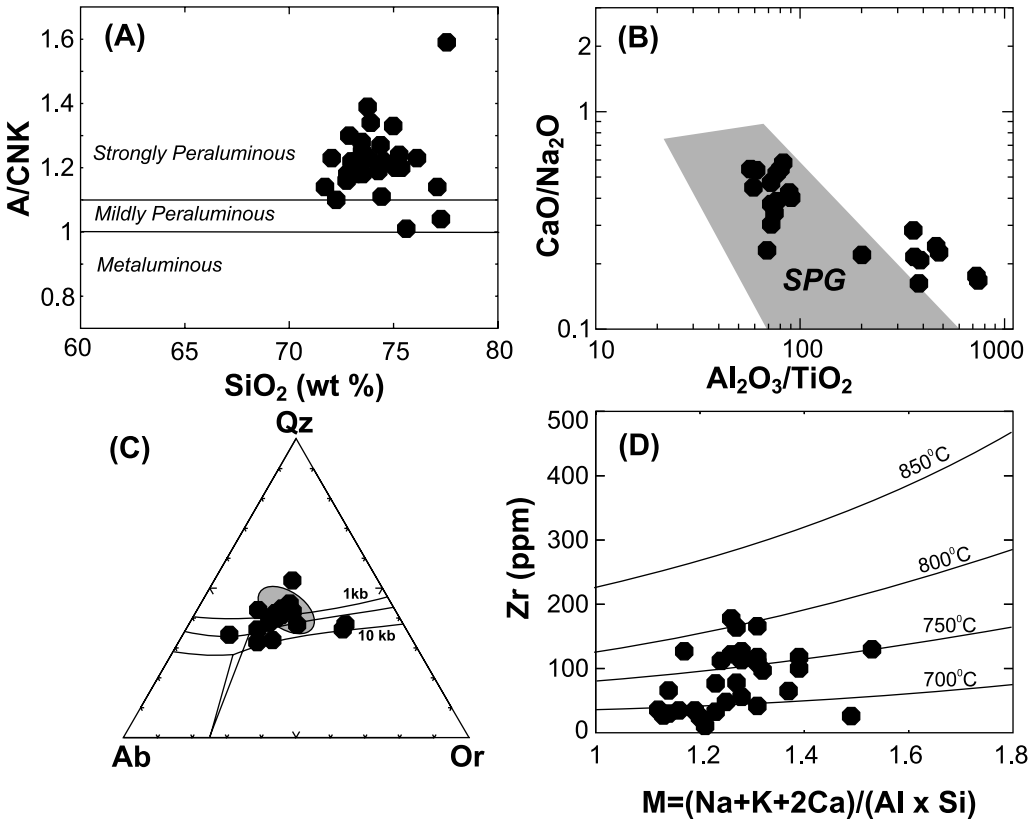

Fig. 3. **A** SiO_2 vs. A/CNK (A/CNK = molar $Al_2O_3/CaO + Na_2O + K_2O$) for the Sikait-Nugrus leucogranites (*Chappell* and *White*, 1974); **B** Al_2O_3/TiO_2 vs. CaO/Na_2O for the Sikait-Nugrus leucogranite; the field of strongly peraluminous granites (SPG) of *Sylvester* (1998) is shown for comparison; **C** CIPW-normative Q–Ab–Or diagram with low temperature melt compositions at 1, 5 and 10 kb (*Johannes* and *Holtz*, 1996), shaded area is the field of two mica leucogranites from the Himalaya (*Visona* and *Lombardo*, 2002); **D** Zr (ppm) vs. M [the cation ratio $(Na + K + 2Ca)/(Al \times Si)$] showing the proportion of Zr that can be dissolved in granitoid melts of various compositions at different temperatures (*Watson* and *Harrison*, 1983)

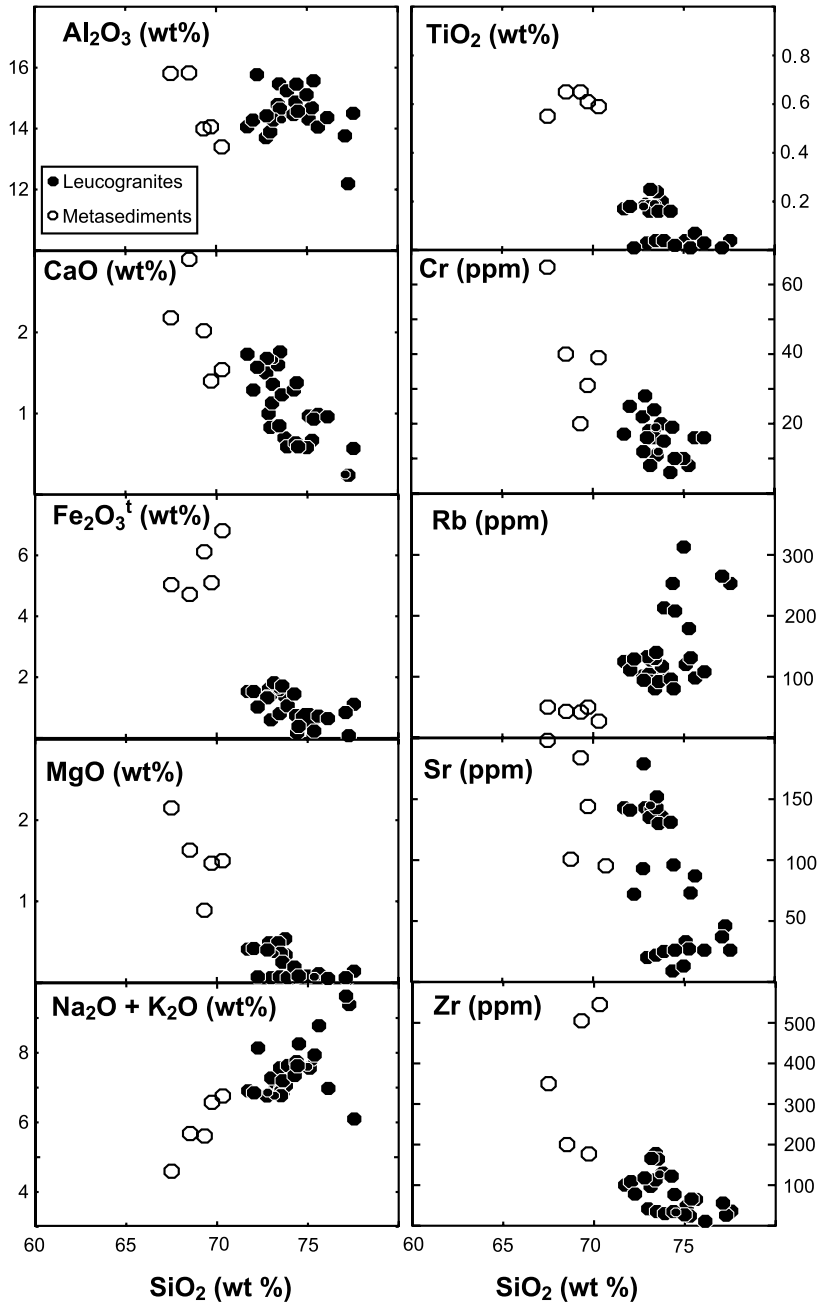

Fig. 4. Harker variation diagrams of some major and trace element contents for the Sikait-Nugrus leucogranite and host metasediments

The REE data (Table 2) and the chondrite-normalized REE diagrams (Fig. 5) show that the leucogranites and the host metasediments display distinct patterns. The metasediments have total REE of 102 to 208 ppm and have REE pattern similar to that of the upper continental crust (*Taylor* and *McLennan*, 1985), with La_N/Yb_N ratios of 9 to 14, moderately fractionated LREE ($La_N/Sm_N = 3 - 5$),

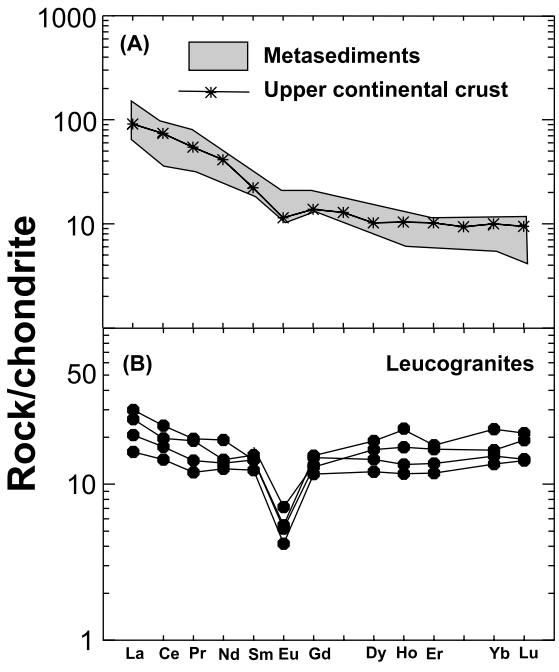

Fig. 5. Chondrite-normalized REE plots (*Sun*, 1982). **A** studied metasediments compared to the upper continental crust (*Taylor* and *McLennan*, 1985). **B** the Sikait-Nugrus leucogranites

weakly fractionated HREE ($Gd_N/Yb_N = 1.4 - 2.3$) and a weak negative Eu anomaly ($Eu/Eu^* = 0.6 - 0.8$). The leucogranites have lower total REE abundances (44–65 ppm) and nearly flat chondrite-normalized patterns (Fig. 5B), with low La_N/Yb_N ratios (1.2–2) and moderate negative Eu anomalies ($Eu/Eu^* = 0.35 - 0.52$). They are characterized by HREE enrichment ($Gd_N/Yb_N = 0.7 - 1$) relative to the metasediments.

Rb–Sr isotope data

$^{87}Rb/^{86}Sr$ and $^{87}Sr/^{86}Sr$ isotopic ratios (Table 3) have been obtained from 13 leucogranite samples and 5 metasediments samples. For the Um Baanib leucogranite, a 5 point whole rock isochron (MSWD = 1.6) yields an age of 610 ± 20 Ma with an initial $^{87}Sr/^{86}Sr$ of 0.7036 ± 0.0004 (Fig. 6A). The 5 analyzed samples from the Um Kheran leucogranite define an age (MSWD = 2.52) of 594 ± 12 Ma and initial $^{87}Sr/^{86}Sr$ of 0.7028 ± 0.0001 (Fig. 6B). The Rb–Sr data for 3 samples of the Sikait leucogranite yields identical model 1 and 3 errochron age (MSWD = 11) of 607 ± 190 Ma and initial $^{87}Sr/^{86}Sr$ of 0.7029 ± 0.0027 (Fig. 6C). Samples from the metasedimentary sequence do not define a meaningful age and scatter around the 610 Ma reference line defined by the Um Baanib leucogranite but at lower $^{87}Rb/^{86}Sr$ (Fig. 6A).

The ages of the different leucogranite bodies appear to reflect either the time of intrusion of the leucogranite or of high-temperature metamorphic overprint. The samples selected for isotope dating are homogeneous with no signs of intense deformation. Thus, the ages obtained probably represent crystallization ages. The initial $^{87}Sr/^{86}Sr$ ratios of the leucogranites vary between 0.7028 and 0.7036,

Table 3. *Rb–Sr isotope data for leucogranites and metasediments*

Sample	Rb	Sr	Rb/Sr	$^{87}Rb/^{86}Sr$	$^{87}Sr/^{86}Sr \pm 2\sigma$
Metasediments					
SD-1	42	184	0.23	0.6605	0.709030 ± 64
SD-2	50	144	0.37	1.0051	0.712130 ± 58
SD-3	27	97	0.28	0.8051	0.711247 ± 64
SD-4	43	108	0.40	1.1580	0.713852 ± 85
SD-5	46	270	0.17	0.4929	0.707690 ± 86
Um Baanib leucogranite					
B842	85	144	0.59	1.7097	0.718425 ± 86
B845	99	143	0.69	2.0057	0.721052 ± 78
B850	123	135	0.91	2.4626	0.724920 ± 90
B858	125	143	0.87	2.5336	0.725850 ± 120
B859	130	153	0.85	2.6410	0.726400 ± 68
Um Kheran leucogranite					
K870	97	152	0.64	1.8485	0.718425 ± 98
K872	7	260	0.03	0.0778	0.703271 ± 42
K881	133	20	6.65	19.5407	0.867010 ± 76
K887	97	145	0.67	1.9375	0.719100 ± 68
K893	94	179	0.53	1.5205	0.715670 ± 44
Sikait leucogranite					
SI-3	108	26	4.15	12.1345	0.806400 ± 96
SI-11	264	46	5.74	16.8355	0.849470 ± 86
S-II-10	129	72	1.79	5.2047	0.748460 ± 102

The 2σ standard error in $^{87}Rb/^{86}Sr$ is 1%. Analytical uncertainties in $^{87}Sr/^{86}Sr$ used to weight the regression and to calculate the MSWD are 0.02%

which indicate that the rocks studied were derived from a juvenile source, and preclude the presence of old continental crust in the study area.

Discussion

Constraints on the source of the leucogranites

Strongly peraluminous leucogranites are commonly associated with regionally metamorphosed and highly folded orogenic belts either along thrust faults and shear zones or they are emplaced as post-tectonic plutons (*Searle* et al., 1997; *Finger* et al., 1997; *Barbarin*, 1999). Various models have been invoked to explain the formation of peraluminous leucogranites. The three most important are: (1) partial melting of quartzo-feldspathic meta-igneous orthogneiss (*Miller*, 1985), (2) reaction between basaltic melts and crustal rocks (*Patiño Douce*, 1995), and (3) the spatial association and the presence of metasedimentary enclaves in the leucogranites, suggest an origin from partial melts of metasedimentary rocks (*Le Fort* et al., 1987; *White* and *Chappell*, 1988; *Barbey* et al., 1990).

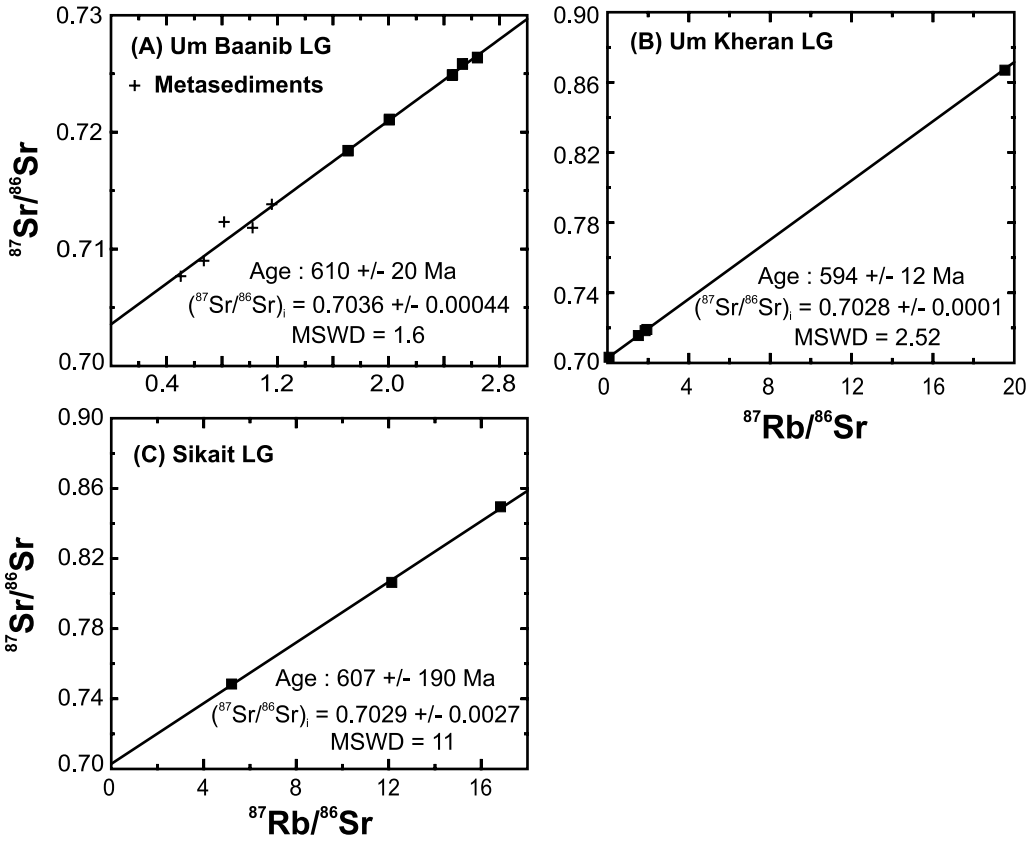

Fig. 6. Whole rock Rb–Sr isochron diagrams for the Sikait-Nugrus leucogranites

Chemical data of the leucogranites investigated that support the hypothesis of crustal melts include: (1) They are strongly peraluminous (Fig. 3A, B) plotting in the low temperature field of the haplogranite Q–Ab–Or system (Fig. 3C), (2) They have chemical composition similar to typical S-type granites (Fig. 7) from the Lachlan Fold Belt (*White* and *Chapell*, 1989) and to melts produced experimentally from metasedimentary rather than metaigneous protoliths (*Patiño Douce* and *Johnston*, 1991; *Vielzeuf* and *Holloway*, 1988), (3) High Rb/Sr (0.53–28.1) and Rb/Ba (0.1–8.7) ratios and the low Sr/Ba ((0.16–1.25) and Rb/Zr (0.5–12) ratios are typical for granites of crustal origin (*Harris* et al., 1986; *Harris* and *Inger*, 1992), (4) The enrichment of Ba (30–929 ppm) and Rb (80–265 ppm) relative to Sr (9–179 ppm), the high K_2O (>3.5%) and low CaO (<2%) indicate a pelitic parent (*Williamson* et al., 1997).

Partial melting of metapelites and quartzo-feldspathic greywacke of suitable compositions and with 1–2 wt% H_2O can generate 15–20% granitic melt at 5 kbar and 700 °C and 30–50% at 5 kbar and 800 °C; these proportions increase with temperature and H_2O content and decrease with pressure (*Clemens* and *Vielzeuf*, 1987). Proportions of volatiles in the analyzed metasediments vary from 1–1.2% and the values of Na_2O, K_2O and SiO_2 occur in proportions suitable for formation of granitic melt. Thus, the metasediments would represent a fertile source for granite magma generation.

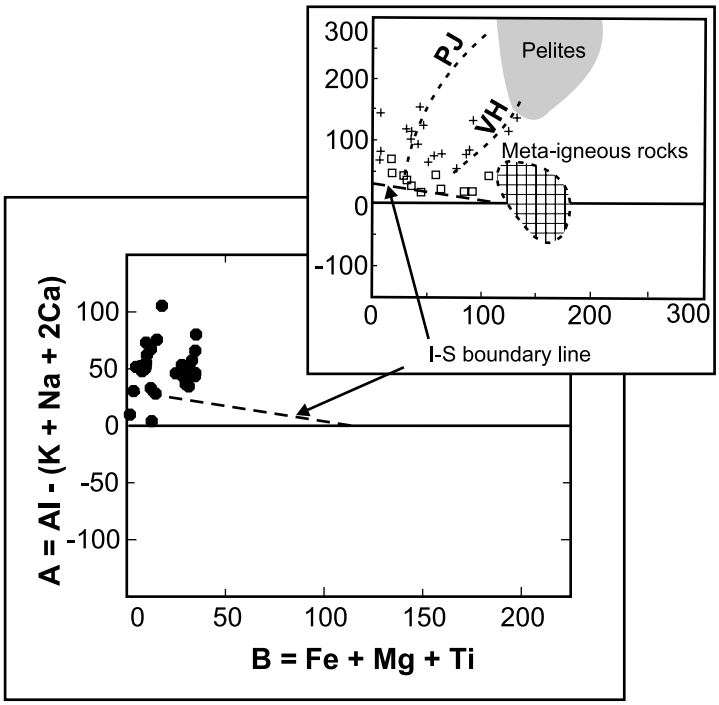

Fig. 7. $A = [Al - (K + Na + 2Ca)]$ vs. $B = (Fe + Mg + Ti)$ binary diagram (*Debon* and *Le Fort*, 1983) for the Sikait-Nugrus leucogranites. I-S line is the boundary between I- and S-type granites (*Villaseca* et al., 1998). Inset shows experimentally derived granitic liquids: (+) = liquids from pelites in different trends with progressive melting (PJ = *Patiño Douce* and *Johnston*, 1991; VH = *Vielzeuf* and *Holloway*, 1988) and (□) = liquids from metaigneous rocks (*Holtz* and *Johannes*, 1991; *Conrad* et al., 1988)

Petrogenesis

Most of the investigated leucogranites have relatively high Al_2O_3/TiO_2 (mainly >70, Fig. 3B), which according to *Sylvester* (1998) indicates low melting temperature. During partial melting of metasediments and at high temperature (>850 °C) nearly all zircon might have been expected to go into solution (*Watson*, 1996). As seen in Fig. 3D, concentrations of Zr are low in the investigated leucogranites suggesting low temperature (<800 °C) for their formation.

As mentioned above, the metasediments in the footwall of the Nugrus fault may represent a fertile source for the Sikait-Nugrus leucogranite magma generation. In Fig. 8A, trace element concentrations of the granites are normalized to the mean of the analyzed metasediments, in order to highlight the changes in chemical composition due to partial melting. For the leucogranites, trace elements that mainly reside in accessory minerals (e.g. Zr, Y, LREE) occur in lower concentrations than observed for the metasediments, indicating that a significant proportion of these elements were retained in the source during anatexis. Trace elements that mainly reside in feldspars and mica (Rb, Ba, Sr) show variable behaviour. Most metasediments have 140–270 ppm Sr, 490–685 ppm Ba, and 27–50 ppm Rb (Table 2). Sr, Ba and Rb concentrations in the granites vary widely; in many leucogranites

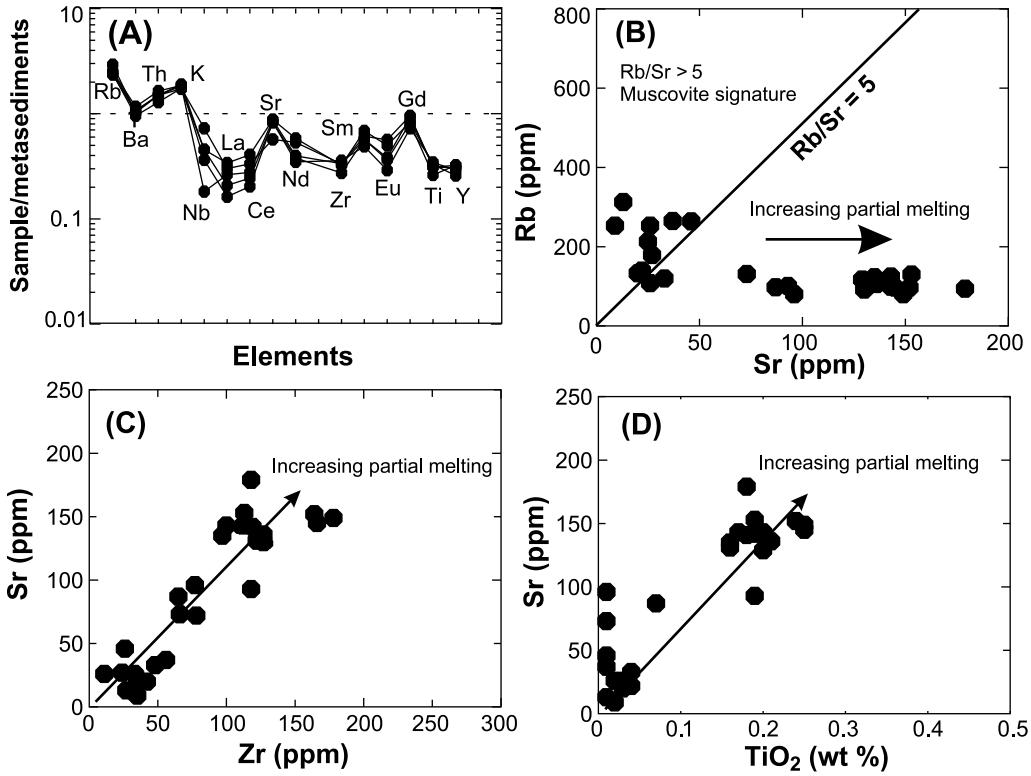

Fig. 8. **A** Incompatible element concentrations in the leucogranites relative to the mean of the metasediments; **B** Sr vs. Rb variation diagram; **C** and **D** Zr vs Sr and TiO_2 vs. Sr variation diagrams for the Sikait-Nugrus leucogranites. The positive correlations between these elements may be related to increasing partial melting of the source rocks

they are similar to those in the metasediments. With increasing Rb there is a decrease in Sr, resulting in high Rb/Sr for some of the samples (Fig. 8B).

Harris et al. (1993) found that high Rb/Sr (10–4) suggests granite formation at vapour-absent conditions (i.e. dehydration melting), whereas Rb/Sr ratios <4 suggest vapour-present melting. Accordingly, it appears that most of the investigated leucogranites (Rb/Sr mostly <4; Fig. 8B) formed by vapour-present melting. Some samples have high Rb/Sr, which suggest local vapour-absent melting. However, the melting experiments of *Holtz* and *Johannes* (1991) show that the addition of H_2O affects CaO/Na_2O and Al_2O_3/TiO_2 in peraluminous melts. With increasing H_2O, CaO/Na_2O increases progressively as the melting point of plagioclase, particularly the anorthite component, decreases. In contrast, Al_2O_3/TiO_2 changes little because biotite stability is not affected by the addition of H_2O. The low CaO/Na_2O (0.12–0.58) and the wide variation in Al_2O_3/TiO_2 (57–1577) in the investigated leucogranites (Table 2, Fig. 3B) suggests their formation by dehydration partial melting according to the melting experiments of *Holtz* and *Johannes* (1991). Moreover, crystallization of the investigated leucogranite from fluid-saturated melt is unlikely because peraluminous granitic melts containing excess H_2O cannot rise far from their source before solidifying. Also, the presence of

euhedral magmatic garnet indicates that the magma was relatively hot and fluid-undersaturated (*Clemens* and *Wall*, 1981; *Vernon* and *Collins*, 1988).

High Rb/Sr (>5) further indicate that some leucogranites were derived by muscovite dehydration melting (*Inger* and *Harris*, 1993; *Harrison* et al., 1999). Conversely, lower Rb/Sr (<4.5) suggests the participation of biotite during melt production of other leucogranite samples. In both leucogranite types, the high contents of Rb reflect biotite and muscovite breakdown (*Icenhower* and *London*, 1996). However, biotite is a more important constituent in the metasediments suggesting that the production of leucogranitic melts involved significant amounts of biotite. The reason for high Rb/Sr in some samples (criterion for muscovite dehydration melting) may reflect increasing temperature during partial melting. In prograde low-pressure metamorphism, the minimum melting reaction for pelites is crossed slightly before dehydration melting of biotite (*Spear* et al., 1999), producing melts with low TiO_2. As partial melting proceeds, not only Ti but also compatible trace elements, such as Sr and Zr contribute towards enriching the melt (*Visona* and *Lombardo*, 2002). The strong positive correlation between Zr vs. Sr and TiO_2 vs. Sr in the leucogranites (Fig. 8C, D) is best explained by different degrees of partial melting due to increasing temperature.

In conclusion, the leucogranites are ascribed to biotite dehydration melting during prograde metamorphism of metasediments.

Tectonic setting and regional geodynamic significance

Neoproterozoic structural evolution in the ANS was complex. There are two main orogenic stages in the geotectonic evolution of the Shield: 1) a principal long-lived stage from ca. 870 Ma to ~ 650 Ma is represented by widespread belts with oceanic affinity. The sequence of events begins with sea-floor spreading and formation of arc and back-arc basins and continues with the accretion of these cells into juvenile crust (*Stern*, 1994). 2) The second stage is relatively short-lived (650–550 Ma) and is represented by belts with continental affinity. Deformation and metamorphism during the second stage occur mainly between 620 and 650 Ma and have been interpreted as a probable collisional stage during which the accreted Pan-African terranes were attached to the East Saharan Craton (*Schandelmeier* et al., 1987; *Kröner* et al., 1994; *Sultan* et al., 1994; *Finger* and *Helmy*, 1998). This collision event is coeval with the collision between East and West Gondwanaland (*Stern*, 1994). Extension at the Neoproterozoic-Cambrian boundary followed collision in the ANS and is related to initial disruption of the Gondwana continent (*Stern*, 1994; *Blasband* et al., 2000; *Fritz* et al., 2002). The major ca. 630–540 Ma Najd fault system formed during extension and related faulting and deformation (*Stern*, 1985; *Sultan* et al., 1993).

We have demonstrated that the leucogranites occur as lens-like bodies along faults, they are mildly deformed along their margins and their emplacement ages are between 594 and 610 Ma, This means that they were formed during extension that follows continental collision (i.e. late tectonic). *Fritz* et al. (1996) show that the Hafafit core complex in the Eastern Desert was cooled below 550 °C at ca. 580 Ma and correlated this with an extensional stage. This presents an additional argument for the emplacement of the leucogranites in an extension-related late tectonic

environment. In the Eastern Desert of Egypt, there is further evidence for extensional tectonics prevailing during the emplacement of the leucogranites: molasse basin formation, emplacement of large masses of post-orogenic A-type granites and Dokhan Volcanics, exhumation of metamorphic core complexes, formation of the major Najd strike-slip fault systems (*Greiling* et al., 1994; *Fritz* et al., 1996; *Moghazi*, 2003; *Jarrar* et al., 2003).

Extensional tectonics following continental collision could have contributed to the generation of crustal-derived granitic melts along shear zones through: 1) partial melting of metasedimentary rocks by decompression of over-thickened crust (*Le Fort* et al., 1987; *Searle* et al., 1997), 2) fluid focusing along crustal shear zones (*Strong* and *Hanmer*, 1981; *Kalsbeek* et al., 2001), and 3) conduction of mantle-derived heat into the lower crust (*Wickham* and *Oxburgh*, 1987). However, the recognition that dehydration melting formed the leucogranites investigated suggests that melting was most probably induced by decompression via slip along shear zones. The concomitant rise of magmatic rocks to shallow crustal levels in addition to fluxing of volatiles along shear zones may have also been a factor in promoting partial melting.

Conclusions

(1) Garnet-bearing leucogranites are locally developed along thrust faults in the Sikait-Nugrus area. They intruded low-grade metamorphosed mélange rocks in the hangingwall of the Nugrus thrust and high-grade metamorphosed sediments (mainly of biotite schist composition) in the footwall of the Nugrus thrust. The leucogranites contain numerous mica schist enclaves.
(2) Major and trace element composition (high SiO_2, A/CNK, Rb/Sr, Rb/Ba and Ba/Sr) and the Rb/Sr isotope data of the leucogranites are consistent with their formation by biotite dehydration melting of juvenile crustal rocks similar to the metasedimentary rocks in the footwall of the major Nugrus thrust.
(3) Geochronological constraints show that the emplacement ages of the leucogranites in the study area are between 594 ± 12 and 610 ± 20 Ma, respectively. Emplacement of leucogranites is probably related to late Neoproterozoic extension following continental collision.
(4) Thermal models consistent with an intracrustal origin of the leucogranites involve crustal heating due to decompression via slip along shear zones of an extending crust.
(5) Whatever the thermal history adopted for the generation of the investigated leucogranites, it seems that they mark a tectonic event within the crust in the Eastern Desert. This event is characterized by late Neoproterozoic crustal extension that follows continental collision and is probably related to the initial break-up of the Gondwana continent.

Acknowledgments

The authors express their thanks to Prof. *Fujimaki* and Dr. *Ishikawa*, Tohoku, Japan, for kindly giving the opportunity to use the XRF and electron microprobe. Thanks are also due to Dr. *T. Oberthür*, Hannover, Germany for REE analyses with ICP-MS. Profs. *R. Stern,*

H. Fritz, and Editor *J. G. Raith* are acknowledged for their valuable and constructive reviews and editorial input that greatly improved the manuscript.

References

Abd El-Naby HH, Frisch W (2002) Origin of the Wadi Haimur-Abu Swayel gneiss belt, south Eastern Desert, Egypt: petrological and geochemical constraints. Precamb Res 113: 307–322

Abdelsalam MG, Liegeois JP, Stern RJ (2002) The Saharan Metacraton. J Afr Earth Sci 34: 119–136

Akaad MK, Noweir AM (1980) Geology and lithostratigraphy of the Arabian Desert orogenic belt of Egypt between latitudes 25° 35′ and 26° 30′N. Inst Appl Geol Jeddah Bull 3: 127–135

Barbarin B (1999) A review of the relationships between granitoid types, their origins and their geodynamic environments. Lithos 46: 605–626

Barbey P, Macaudiere J, Uzenti JP (1990) High-pressure dehydration melting of metapelites: evidence from migmatites of Yaoundi (Cameroon). J Petrol 31: 401–428

Bennett JD, Mosley PN (1987) Tiered-tectonics and evolution, Eastern Desert and Sinai, Egypt. In: *Matheis G*, *Schandelmeier H* (eds) Current research in African earth sciences. Balkema, Rotterdam, pp 79–82

Beyth M, Stern RJ, Altherr R, Kröner A (1994) The late Precambrian Timna igneous complex, southern Israel: evidence for comagmatic-type sanukitoid monzodiorite and alkali granite magma. Lithos 31: 103–124

Blasband B, White S, Brooijmans B, De Boorder H, Visser W (2000) Late Proterozoic extensional collapse in the Arabian-Nubian Shield. J Geol Soc Lond 157: 615–628

Bregar M, Bauernhofer A, Pelz K, Kloetzli U, Fritz H, Neumayr P (2002) A late Neoproterozoic magmatic core complex in the Eastern Desert of Egypt: emplacement of granitoids in a wrench-tectonic setting. Precamb Res 118: 59–82

Chappell BA, White AJR (1974) Two contrasting granite types. Pacific Geol 8: 173–174

Clemens JD, Vielzeuf D (1987) Constraints on melting and magma production in the crust. Earth Planet Sci Lett 86: 287–306

Clemens JD, Wall VJ (1981) Crystallization and origin of some peraluminous (S-type) granitic magmas. Can Mineral 19: 111–132

Conrad WK, Nicholls IA, Wall VJ (1988) Water-saturated and undersaturated melting of metaluminous and peraluminous crustal composition at 10 kb: evidence for the origin of silicic magmas in the Taupo Volcanic Zone, New Zealand, and other occurrences. J Petrol 29: 765–803

Debon F, Le Fort P (1983) A chemical-mineralogical classification of common plutonic rocks and their magmatic associations. Trans Roy Soc Edinburgh, Earth Sci 73: 135–149

El Gaby S, List FK, Tehrani R (1990) The basement complex of the Eastern Desert and Sinai. In: *Said R* (ed) The geology of Egypt. Balkema, Rotterdam, pp 175–184

El Ramly MF, Greiling R, Kröner A, Rashwan AA (1984) On the tectonic evolution of the Wadi Hafafit area and environs, Eastern Desert of Egypt. Inst Appl Geol Jeddah Bull 6: 113–146

Finger F, Helmy HM (1998) Composition and total-Pb model ages of monazite from high-grade paragneisses in the Abu Swayel area, south Eastern Desert, Egypt. Mineral Petrol 62: 269–289

Finger F, Roberts MP, Haunschmid B, Schermaier A, Steyrer HP (1997) Variscan granitoids of central Europe: their typology, potential sources and tectonothermal relations. Mineral Petrol 61: 67–96

Fowler A, El Kalioubi B (2002) The Migif-Hafafit gneissic complex of the Egyptian Eastern Desert: fold interference patterns involving multiply deformed sheath folds. Tectonophysics 346: 247–275

Fowler TJ, Osman AF (2001) Gneiss-cored interference dome associated with two phases of late Pan-African thrusting in the central Eastern Desert, Egypt. Precamb Res 108: 7–43

Fritz H, Wallbrecher E, Khudeir AA, Abu El Ela FF, Dallmeyer DR (1996) Formation of Neoproterozoic metamorphic core complexes during oblique convergence (Eastern Desert, Egypt). J Afr Earth Sci 23: 311–329

Fritz H, Dallmeyer DR, Wallbrecher E, Loizenbauer J, Hoinkes G, Neumayr P, Khudeir AA (2002) Neoproterozoic tectonothermal evolution of the Central Eastern Desert, Egypt: a slow velocity tectonic process of core complex exhumation. J Afr Earth Sci 34: 137–155

Greiling RO, Kröner A, El-Ramly MF, Rashwan AA (1988) Structural relationships between the southern and central parts of the Eastern Desert of Egypt: details of a fold and thrust belt. In: *El-Gaby S, Greiling RO* (eds) The Pan-African belt of Northeast Africa and adjacent areas. Vieweg, Wiesbaden, pp 121–146

Greiling RO, Abdeen MM, Dardir AA, El-Akhal H, El-Ramly MF, Kamal El-Din GM, Osman AF, Rashwan AA, Rice AHN, Sadek MF (1994) A structural synthesis of the Proterozoic Arabian–Nubian Shield in Egypt. Geol Rundsch 83: 484–501

Harris NB, Inger S (1992) Trace element modelling of pelite-derived granites. Contrib Mineral Petrol 110: 46–56

Harris NB, Pearce JA, Tindle AG (1986) Geochemical characteristics of collision zone magmatism. In: *Conward MP, Ries AC* (eds) Collision tectonics. Spec Publ Geol Soc Lond 19: 67–81

Harris N, Inger S, Massey J (1993) The role of fluids in the formation of High Himalayan leucogranites. In: *Treloar PJ, Searle MP* (eds) Himalayan tectonics. Spec Publ Geol Soc Lond 74: 391–400

Harrison TM, Grove M, McKeegan KD, Coath CD, Lovera OM, Le Fort P (1999) Origin and episodic emplacement of the Manaslu intrusive complex, central Himalaya. J Petrol 40: 3–19

Hassan MA, Hashad AH (1990) Precambrian of Egypt. In: *Said R* (ed) The geology of Egypt. Balkema, Rotterdam, pp 201–245

Hilmy ME, El Bayoumi RM, Eid AS (1990) Geology, geochemistry and mineralization of the psammitic gneiss of the Wadi Abu Rusheid, Eastern Desert, Egypt. J Afr Earth Sci 11: 197–205

Holtz F, Johannes W (1991) Genesis of peraluminous granites. I. Experimental investigation of melt compositions at 3 and 5 kb and various H_2O activities. J Petrol 32: 935–958

Icenhower J, London D (1996) Experimental partitioning of Rb, Cs, Sr, and Ba between alkali feldspar and peraluminous melt. Am Mineral 81: 719–734

Inger S, Harris N (1993) Geochemical constraints on leucogranite magmatism in the Lantang valley, Nepal Himalaya. J Petrol 34: 345–368

Jarrar G, Stern RJ, Saffarini G, Al Zubi H (2003) Late- and post-orogenic Neoproterozoic intrusions of Jordan: implications for crustal growth in the northernmost segment of the East African Orogen. Precamb Res 123: 295–319

Johannes W, Holtz F (1996) Petrogenesis and experimental petrology of granitic rocks. Minerals and Rocks 22. Springer, Berlin Heidelberg New York Tokyo, 335 pp

Kalsbeek F, Jepsen HF, Nutman AP (2001) From source migmatites to plutons: tracking the origin of c. 435 Ma S-type granites in the East Greenland Caledonian orogen. Lithos 57: 1–21

Kröner A (1985) Ophiolites and the evolution of tectonic boundaries in the late Proterozoic Arabian–Nubian Shield of Northeast Africa and Arabia. Precamb Res 27: 235–257

Kröner A, Reischmann T, Wust H-J, Rashwan AA (1988) Is there any pre-Pan-African (>950 Ma) basement in the Eastern Desert of Egypt. In: *El Gaby S, Greiling RO* (eds) The Pan-African belt of northeast Africa and adjacent areas. Vieweg, Braunschweig, pp 93–119

Kröner A, Todt W, Hussein IM, Mansour M, Rashwan AA (1992) Dating of late Proterozoic ophiolites in Egypt and the Sudan using the single grain zircon evaporation technique. Precamb Res 59: 15–32

Kröner A, Krüger J, Rashwan AA (1994) Age and tectonic setting of granitoid gneisses in the Eastern Desert of Egypt and south–west Sinai. Geol Rundsch 83: 502–513

Le Fort P, Cuney M, Deniel C, France-Lanord C, Sheppard SMF, Upreti BN, Vidal P (1987) Crustal generation of the Himalayan leucogranites. Tectonophysics 134: 39–57

Loizenbauer J, Wallbrecher E, Fritz H, Neumayr P, Khudeir AA, Kloetzli U (2001) Structural geology, single zircon ages and fluid inclusion studies of the Meatiq metamorphic core complex: implications for Neoproterozoic tectonics in the Eastern Desert of Egypt. Precamb Res 110: 357–383

Ludwig KR (1991) ISOPLOT: a plotting and regression program for radiogenic isotope data. Version 2.75. US Geol Surv, Open File Report, pp 91–445

Meert JG (2003) A synopsis of events related to the assembly of eastern Gondwana. Tectonophysics 362: 1–40

Miller CF (1985) Are strongly peraluminous magmas derived from pelitic sedimentary rocks? J Geol 93: 673–689

Moghazi AM (1999) Magma source and evolution of late Neoproterozoic granitoids in the Gabal El Urf area, Eastern Desert, Egypt: geochemical and Sr–Nd isotopic constraints. Geol Mag 136: 285–300

Moghazi AM (2003) Geochemistry and petrogenesis of a high-K calc–alkaline Dokhan Volcanic Suite, South Safaga area, Egypt: the role of late Neoproterozoic crustal extension. Precamb Res 125: 161–178

Moghazi AM, Hassanen MA, Hashad MH, Mohamed FH (2001) Garnet-bearing leucogranite in the El Hudi area, southern Egypt: evidence of crustal anatexis during Pan-African low pressure regional metamorphism. J Afr Earth Sci 33: 245–259

Mohamed FH, Hassanen MA (1997) Geochemistry and petrogenesis of Sikait leucogranite, Egypt: an example of S-type granite in a metamorphic sequence. Geol Rundsch 86: 81–92

Patiño Douce AE (1995) Experimental generation of hybrid silicic melts by reaction of high Al basalt with metamorphic rocks. J Geophys Res 100: 623–639

Patiño Douce AE, Johnston AD (1991) Phase equilibria and melt productivity in the pelitic system: implications for the origin of peraluminous granitoids and aluminous granulites. Contrib Mineral Petrol 107: 202–218

Ragab AI, El-Gharabawi RI (1989) Wadi El-Hudi migmatites, East of Aswan, Egypt: a geological study and some geotectonic implications for the Eastern Desert of Egypt. Precamb Res 44: 67–79

Rashwan AA (1991) Petrography, geochemistry and petrogenesis of the Migif-Hafafit Gneisses at Hafafit Mine area, Egypt. Scientific Series of the International Bureau: Forschungszentrum Jülich GmbH 5: 359 pp

Schandelmeier H, Richter A, Harms U (1987) Proterozoic deformation of the East Saharan Craton in southeast Libya, south Egypt and north Sudan. Tectonophysics 140: 233–246

Searle MP, Parrish RR, Hodges KV, Hurford A, Ayres MW, Whitehouse MJ (1997) Shisha Pangma leucogranite, south Tibetan Himalaya: field relations, geochemistry, age, origin, and emplacement. J Geol 105: 295–317

Spear F, Kohn M, Cheney J (1999) P-T paths from anatectic pelites. Contrib Mineral Petrol 134: 17–32

Stern RJ (1985) The Najd Fault System, Saudi Arabia and Egypt: a late Precambrian rift-related transform system? Tectonics 4: 497–511

Stern RJ (1994) Arc assembly and continental collision in the Neoproterozoic East African Orogen: implications for the consolidation of Gondwanaland. Ann Rev Earth Planet Sci 22: 319–351

Stern RJ (2002) Crustal evolution in the East African Orogen: a neodymium isotopic prospective. J Afr Earth Sci 34: 109–117

Stern RJ, Gottfried D (1986) Petrogenesis of late Precambrian (575–600 Ma) bimodal suite in northeast Africa. Contrib Mineral Petrol 92: 492–501

Stern RJ, Hedge CE (1985) Geochronologic and isotopic constraints on late Precambrian crustal evolution in the Eastern Desert of Egypt. Am J Earth Sci 285: 97–127

Stern RJ, Manton WI (1987) Age of Feiran basement rocks, Sinai: implications for late Precambrian crustal evolution in the northern Arabian-Nubian Shield. J Geol Soc Lond 144: 569–575

Strong DF, Hanmer SK (1981) The leucogranites of southern Brittany: origin by faulting, frictional heating, fluid flux and fractional melting. Can Mineral 19: 163–176

Sturchio NC, Sultan M, Batiza R (1983) Geology and origin of Meatiq dome, Egypt: a Precambrian metamorphic core complex. Geology 11: 72–76

Sultan M, Bickford ME, El Kaliouby B, Arvidson RE (1992) Common Pb systematics of Precambrian granitic rocks of the Nubian Shield (Egypt) and tectonic implications. Geol Soc Am Bull 104: 456–470

Sultan M, Becker R, Arvidson RE, Shore P, Stern RJ, El Alfy Z, Attia RI (1993) New constraints on Red Sea rifting from correlation of Arabian and Nubian Neoproterozoic outcrops. Tectonics 12: 1303–1319

Sultan M, Tucker RD, El Alfy Z, Attia R, Ragab AG (1994) U–Pb (zircon) ages for the gneissic terrane west of the Nile, southern Egypt. Geol Rundsch 83: 514–522

Sun S-S (1982) Chemical composition and origin of the Earth's primitive mantle. Geochim Cosmochim Acta 46: 179–192

Sylvester PJ (1998) Post-collisional strongly peraluminous granites. Lithos 45: 29–44

Takla MA, Basta FF, Surour AA (1992) Petrology and mineral chemistry of rodingites associating the Pan-African ultramafics of Sikait-Abu Rusheid area, south Eastern Desert, Egypt. 1st Conference on Geology of the Arab World, Cairo University, Cairo, pp 491–507

Taylor SR, McLennan, SM (1985) The continental crust: its composition and evolution. Blackwell, Oxford, 312 pp

Vernon RH, Collins WJ (1988) Igneous microstructures in migmatites. Geology 16: 1126–1129

Vielzeuf D, Holloway J (1988) Experimental determination of the fluid-absent melting relations in the pelitic system. Contrib Mineral Petrol 98: 257–276

Villasecca C, Barbero L, Rogers G (1998) Crustal origin of Hercynian peraluminous granitic batholiths of Central Spain: petrological, geochemical and isotopic (Sr, Nd) constraints. Lithos 43: 55–79

Visona D, Lombardo B (2002) Two-mica and tourmaline leucogranites from the Everest–Makalu region (Nepal–Tibet). Himalayan leucogranite genesis by isobaric heating? Lithos 62: 125–150

Wallbrecher E, Fritz H, Khudeir AA, Farahad F (1993) Kinematics of Panafrican thrusting and extension in Egypt. In: *Thorweihe U, Schandelmeier H* (eds) Geoscientific research in Northeast Africa. Balkema, Rotterdam, pp 27–30

Watson E (1996) Dissolution, growth, and survival of zircons during crustal fusion: kinetic principles, geological models and implications for isotopic inheritance. Trans Roy Soc Edinburgh, Earth Sci 87: 43–56

Watson E, Harrison TM (1983) Zircon saturation revisited: temperature and composition effects in a variety of crustal magma types. Earth Planet Sci Lett 64: 295–304

White AJR, Chappell BW (1988) Some supracrustal S-type granites of the Lachlan Fold Belt. Trans Roy Soc Edinburgh, Earth Sci 79: 169–181

White AJR, Chappell BW (1989) Geology of the Numbla. 1:100,000 Sheet 8624 . Geol Surv NSW, Sydney

Wickham SM, Oxburgh ER (1987) Low-pressure regional metamorphism in the Pyrenees and its implications for the thermal evolution of rifted continental crust. Trans Roy Soc Lond A 321: 219–242

Williamson BJ, Downes H, Thirlwall MF, Beard A (1997) Geochemical constraints on restite composition and unmixing in the Velay anatectic granite, French Massif Central. Lithos 40: 295–319

Willis KM, Stern RJ, Clauer N (1988) Age and geochemistry of late Precambrian sediments of the Hammamat series from the Northeastern Desert of Egypt. Precamb Res 42: 173–187

Authors' addresses: *A.M. Moghazi* (corresponding author; e-mail: moghazi_16@yahoo.com), *M.A. Hassanen* and *F.H. Mohamed*, Geology Department, Faculty of Science, Alexandria University, Alexandria, Egypt; *S. Ali*, Faculty of Earth Sciences, King Abdulaziz University, Jeddah, Saudi Arabia